Analytic Model for the Dipole Potential of a Lipid Layer

Klemen Bohinc,*,[†] Juan J. Giner-Casares,[‡,§] and Sylvio May[∥]

[†]Faculty of Health Sciences, University of Ljubljana, Zdravstvena 5, SI-1000 Ljubljana, Slovenia

[‡]BioNanoPlasmonics Lab, CIC biomaGUNE, 20009 Donostia - San Sebastian, Spain

[§]Department of Physical Chemistry and Applied Thermodynamics, University of Cordoba, Campus de Rabanales, Edificio Marie Curie, Cordoba E-14014, Spain

[∥]Department of Physics, North Dakota State University, Fargo, North Dakota 58108-6050, United States

ABSTRACT: The larger permeability of anions than cations through a lipid bilayer can be rationalized by the positive sign of the bilayer's dipole potential. That is, upon crossing the lipid headgroups toward the hydrocarbon chain region, the electrostatic potential increases by several hundred millivolts. We derive an analytic expression for the dipole potential of a single lipid layer using an electrostatic model that is based on an extended version of the linearized Poisson−Boltzmann theory. The model highlights the ability of the lipid headgroups to render the dipole potential positive by inducing an orientational ordering of the solvent molecules. The positive contribution of the solvent overcompensates the negative dipole potential due to the bare lipids. Our theoretical prediction compares accurately with measurements of the dipole potential that we have conducted for mixed anionic−zwitterionic lipid monolayers at the air−water interface.
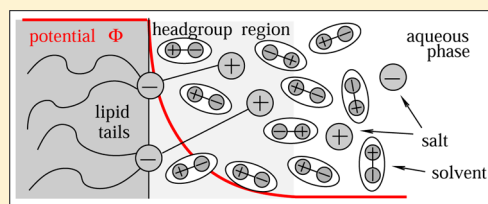
INTRODUCTION

One of the lipid's most basic functions in a biomembrane is to compartmentalize space and allow for protein-mediated regulation of ion permeabilities by forming a self-assembled and highly impermeable barrier for hydrophilic and charged molecules. It is well-known that anions tend to diffuse through a model membrane faster than cations. More then 40 years ago, Lieberman and Topaly[1] as well as LeBlanc[2] proposed that the observed permeability differences can be explained by a positive sign of the electrostatic potential in the interior of the bilayer as compared to the aqueous solution. Multiple molecular origins for the positive sign of this so-called *dipole potential* have been suggested and discussed.[3,4] Most notable are oriented water molecules in the vicinity of the bilayer headgroup region,[5,6] the ester groups that link the headgroup to the glycerol backbone,[7] and fatty acid carbonyl groups of the lipids.[8] In contrast, contributions from the methylene groups of the fatty acid chains are likely to be minor.[9,10] It has been pointed out that the observed permeability differences between cations and anions may not only originate exclusively from the membrane's dipole potential but also from variations in effective ion sizes due to different hydration patterns of cations versus anions.[11]

Experimental results agree about the positive sign of the dipole potential but vary significantly with regard to its magnitude.[4,9,12,13] Membrane conductance and surface potential measurements suggest that the dipole potential of lipid monolayers composed of phosphatidylcholines with varying chain length and saturation is about 300−400 mV.[14] Transport measurements of hydrophobic ions across planar bilayers and vesicles estimate a dipole potential in the range 200−300 mV.[15] The direct electrochemical method developed by Becucci et al.[16] yields a dipole potential of about 145 mV for neutral

dioleoylphospholipids. Using atomic force microscopy, Yang et al.[17] measured a repulsive force between a negatively charged probe tip and a supported phosphatidylcholine bilayer, which resulted from the electrostatic field created by a positive membrane dipole potential of 275 mV. The magnitude of the dipole potential decreases if the fatty acid carbonyl groups in the ether lipid are not present.[18] Wang et al.[19] introduced a cryo electron microscopy method that uses electrons to directly measure the dipole potential of rapidly frozen lipid membranes. The dipole potential was estimated to be 510 mV for an ester lipid as opposed to 260 mV for the corresponding ether lipid.

The decisive role that membrane-induced ordering of water molecules plays for both the magnitude and sign of its dipole potential has been revealed by a multitude of atomistic[20−22] and united atom[23,24] molecular dynamics (MD) simulations as well as by a number of computational mean-field electrostatic calculations.[25−27] What these computer-based modeling approaches suggest is that the bare lipids provide a negative contribution to the dipole potential. This is perhaps no surprise because the negatively charged phosphate groups of typical phospholipids such as phosphatidylcholine reside on average closer to the hydrocarbon chain region than the positively charged choline group. However, the negative contribution from the bare lipids is overcompensated by a positive contribution of oriented water molecules that are associated with the lipid headgroup.[28−31] Hence, headgroup-induced ordering of the solvent molecules appears to be crucial for the net dipole potential to be positive.[32,33] Clearly, if all water

molecules are treated as a continuum dielectric medium, both the sign and magnitude of the dipole potential will be incorrect.[34]

Classical Poisson–Boltzmann (PB) theory[35,36] is a frequently used mean-field approach to characterize ion distributions near charged surfaces, including lipid membranes. Indeed, the PB model has been used to numerically compute electrostatic potentials using atomistic models for lipids.[34,37,38] However, the PB model is also appealing due to its ability to predict certain analytical solutions of electrostatic potentials near charged surfaces.[39] The continuum PB approach, including its linearized Debye–Hückel limit, has evolved into a valuable tool for understanding a multitude of electrostatic phenomena such as counterion condensation[40] and counterion release in biopolymer–membrane interactions.[41] The classical continuum PB model neglects all charge–charge correlations[42] and treats the solvent strictly as a dielectric background. On this level, neither the lipid-induced ordering of water molecules nor any molecular details of the lipid structure (including the spatial distribution of headgroup charges and conformational degrees of freedom of the headgroup) are accounted for. However, there has been recent progress in incorporating both the dipolar nature of zwitterionic headgroups[43–45] and the presence of solvent molecules[46–51] explicitly into the PB formalism. This suggests (and has motivated us) to address the problem of modeling the dipole potential across a lipid layer within the framework of the continuum PB approach.

The present work proposes an electrostatic model for the dipole potential of a mixed anionic–zwitterionic lipid layer. To this end, we employ the linearized (Debye–Hückel) limit of an extended continuum PB model that accounts for the dipolar nature of the zwitterionic headgroups and explicitly treats the solvent molecules as orientationally adjustable dipoles. Our goal is to derive simple closed-form expressions for all physically relevant parameters, including the dipole potential, from functional minimization of a free energy expression. Our model combines two opposing structural features, the intrinsic dipolar nature of a bare zwitterionic headgroup (which tends to render the dipole potential more negative), and the ability of the lipids to orientationally order solvent molecules in the vicinity of the lipid headgroup region (which provides a positive contribution to the dipole potential). In order to compare our model to experimental data, we have measured the potential difference across a lipid monolayer at the air–water interface for different mixtures of anionic and zwitterionic lipids. We demonstrate that our analytic model is able to reproduce both the sign and magnitude of the measured dipole potential, including its dependencies on the monolayer composition and average molecular area per lipid.

MATERIALS AND METHODS

Dimyristoylphosphatidylcholine (DMPC) and L-α-dimyristoyl-phosphatidic acid (DMPA) were purchased from Fluka and used as received. A mixture of chloroform and methanol at a ratio of 3:1 (v/v) was used as the spreading solvent for dissolving both components. The pure solvents were obtained and used without purification from Aldrich. Ultrapure water, produced by a Millipore Milli-Q unit, pretreated by a Millipore reverse osmosis system (>18.2 MΩ cm), was used as a subphase. The subphase temperature was 21 °C at pH 5.7.

A Nima 611D Langmuir trough with one moving barrier (Nima Technology, Coventry, England) was used and provided with a Wilhelmy-type dynamometric system using a strip of filter paper. The surface potential at the air–water interface was measured with a surface-potential probe equipped with a vibrating plate (Kelvin Probe SP1, Accurion Technologies, Göttingen, Germany). The variation of the monolayer surface potential was obtained at the same time as the surface pressure–molecular area isotherm. The monolayers were compressed at a speed of ca. 0.1 nm^2 min^{-1} molecule^{-1}. All measurements have been performed at least three times, showing good reproducibility. No dependence on the number of molecules spread on the interface versus mean molecular area was observed.

EXPERIMENT

Employing the surface potential Kelvin method,[4,28] we measured the potential difference induced by a lipid monolayer,[52] consisting of dimyristoylphosphatidylcholine (DMPC) and L-α-dimyristoylphosphatidic acid (DMPA), at the air–water interface as a function of the average molecular area per lipid a. The corresponding lateral pressure π and lipid-induced dipole potential Φ_{dip} are shown in Figure 1 for four
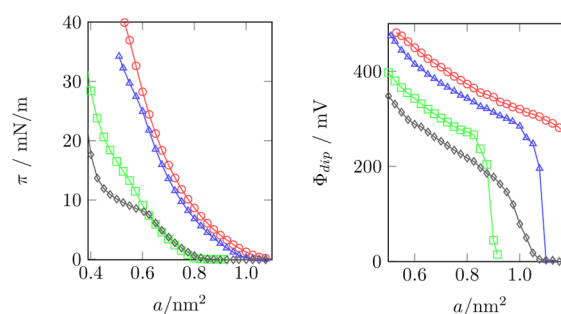

Figure 1. Lateral pressure π of a mixed DMPC/DMPA monolayer (left diagram) and corresponding dipole potential Φ_{dip} (right diagram) as a function of the molecular area a per lipid. Different curves refer to different mole fractions ϕ of DMPA: $\phi = 0$ (red curve), $\phi = 0.25$ (blue curve), $\phi = 0.5$ (green curve), and $\phi = 1$ (black curve).

different compositions, corresponding to the mole fractions $\phi = 0$ (red), $\phi = 0.25$ (blue), $\phi = 0.5$ (green), and $\phi = 1$ (black), of DMPA. As is well-known from similar previous studies,[28] the dipole potential is positive and decreases with increasing a. The measured potential differences in the liquid-expanded phase are, roughly, between 500 and 200 mV for molecular lipid areas between 0.50 and 0.80 nm^2. Our experimental data are in close agreement with previous results.[14,28]

Note that for 0.5 nm$^2 \leq a \leq 0.9$ nm^2 the observed change of Φ_{dip} is approximatively linear in composition ϕ. However, the observed linear dependence may not necessarily reflect the actual composition dependence of the dipole potential on a molecular level. In particular, if the mixed monolayer undergoes phase separation, the observed dipole potential is the composition-weighted average of the dipole potentials of the individual phases. In other words, Φ_{dip} is observed to change linearly with composition, even if the actual change of the dipole potential with composition would be nonlinear for a homogeneously mixed monolayer. Indeed, from experimental and simulation studies of lipid bilayers, it is known that the mixture of DMPC and DMPA is nonideal, leading to lipid clustering and possibly the formation of domains. In particular, low pH (below 4) or the addition of divalent ions such as calcium promotes phase segregation.[53,54] At our experimental conditions (pH of 5.7 and in the absence of divalent cations),

lipid clustering and domain formation are less prevalent.[55] Our theoretical model described below predicts a linear dependence of $\Phi_{dip}(\phi)$. In fact, being a mean-field superposition of the dipole potentials for monolayers consisting of the individual lipids, our model can only predict a linear dependence for $\Phi_{dip}(\phi)$ and thus does not attempt to make predictions beyond those that would be observed for a domain-forming monolayer.

■ THEORY

Our theoretical model of a mixed lipid layer (see the schematic illustration in Figure 2) describes either a monolayer at the air–

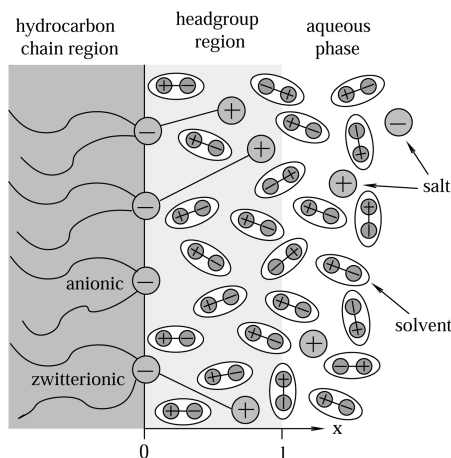**Figure 2.** Schematic illustration of a mixed anionic–zwitterionic lipid layer, which is divided into three regions: the hydrocarbon chain region ($x < 0$), the headgroup region ($0 \leq x \leq l$), and an aqueous phase ($x > l$) that may contain salt. The headgroup region contains anionic and zwitterionic headgroups as well as dipolar solvent molecules. The density of the solvent decreases toward the hydrocarbon chain region, whereas its orientational ordering increases. The position $x = 0$ coincides with the apolar/polar surface.

water interface or one of the two leaflets of a lipid bilayer residing in an aqueous solution.[52] The lipid layer consists of anionic and zwitterionic lipids with mole fractions ϕ and $(1 - \phi)$, respectively, both occupying the same lateral cross-sectional area a. For the zwitterionic headgroup (DMPC in our experiments), we adopt a simple structural model:[43,56] it consists of two point charges of opposite sign, separated by a fixed distance l. The two charges model the P^-–N^+ dipole, namely, the negatively charged phosphate group and the positively charged quaternary ammonium cation of phosphatidylcholine. The phosphate group is linked to the hydrocarbon chains, making the negative charge relatively immobile. In contrast, due to the headgroup's orientational and conformational degrees of freedom, the positive charge exhibits considerable mobility and is thus able to reside at different positions inside the headgroup region. It is reasonable to simply assume that (1) the negative charge is confined to the polar/apolar surface, located at position $x = 0$ along the normal direction (the x-axis) of the lipid layer, and (2) the positive charge is smeared uniformly within the headgroup region, $0 \leq x \leq l$. Note that a uniform charge density along the x-direction would strictly emerge if inside the headgroup region all orientations of the headgroup dipole had the same probability.

In our experiments, the anionic lipid is dimyristoylphosphatidic phosphatidic acid (DMPA), for which the headgroup consists of a single phosphate group, suggesting that we treat

the headgroup of the anionic lipid analogously as a single negative charge located at $x = 0$. Hence, each of the two lipids' phosphate groups makes a contribution $[-(1 - \phi)e/a$ for the zwitterionic and $-\phi e/a$ for the anionic headgroup] to the total surface charge density $\sigma = -e/a$ at $x = 0$, where e denotes the elementary charge.

The second component of our model pertains to the structure of water. We model the aqueous solvent explicitly as an ensemble of dipoles, each consisting of two elementary charges of opposite sign separated by a fixed distance $l_W = 0.1$ nm, implying a dipole moment $p_w = el_W$. The dipoles are able to optimize their orientational distribution as a result of interactions with both the lipids and with the local electrostatic potential. In addition, the solvent density decreases inside the headgroup region, becoming negligibly small when entering the hydrocarbon chain region. This decrease is a result of the headgroups shielding the lipid tails from the unfavorable interaction with the solvent.

For a homogeneously mixed, planar lipid layer of sufficient lateral extension (large lateral area A), all average physical quantities depend only on the x-direction, allowing us to express the area density of the total free energy F (measured in units of the thermal energy k_BT, where k_B is Boltzmann's constant and T the absolute temperature) as

$$\frac{F}{Ak_BT} = \int_0^\infty dx \frac{\Psi'^2}{8\pi l_B} + \int_0^\infty dx \frac{n}{2}(\langle p^2 \rangle - 1)$$
$$+ \lambda \int_0^\infty dx(\langle p \rangle - 1) + \alpha \frac{2l}{l_C} \int_0^l dx \langle sp \rangle n'$$
$$+ \int_l^\infty dx \left\{ \frac{n_+^2}{2n_0} - n_+ + \frac{n_-^2}{2n_0} - n_- \right\} \tag{1}$$

This free energy applies to the weak perturbation regime, known as the linearized Debye–Hückel limit of the classical nonlinear PB theory. The first term in eq 1 corresponds to the energy stored in the electrostatic field, here expressed in terms of the commonly used *dimensionless* electrostatic potential $\Psi = e\Phi/(k_BT)$ instead of the electrostatic potential Φ. Note that $\Phi = \Psi \cdot 25$ mV at room temperature. In eq 1 and below, a prime represents the derivative with respect to x (that is, $\Psi' = d\Psi/dx$, etc.). Because we model the solvent explicitly, the Bjerrum length $l_B = e^2/(4\pi\varepsilon_0 k_BT) = 56$ nm refers to vacuum (ε_0 is the permittivity in vacuum) and room temperature. An effective Bjerrum length of $l_B^W = 0.7$ nm in bulk water will emerge below from our model; see the discussion following eq 9. The second term in eq 1 describes the orientational entropy of the solvent molecules. A given solvent molecule at position x is represented by an orientationally mobile dipole whose instantaneous orientation is characterized by the projected dipole length s along the x-axis and a corresponding (yet unknown) orientational probability distribution $p = p(x, s)$, normalized such that $\langle p \rangle = 1$ in unoriented water (see eq 2 for a formal definition of the orientational average). In eq 1, the expression $p \ln p \approx (p^2 - 1)/2$ for the dipole's orientational entropy contribution represents the small perturbation limit. We define the orientational averaging of any physical quantity $g(s)$ by

$$\langle g \rangle = \frac{1}{l_W} \int_{-l_W/2}^{l_W/2} ds \, g(s) \tag{2}$$

where we recall that l_W is the length of the solvent dipole. The integral in eq 2 extends over all solvent orientations.

Orientational averaging over the probability distribution $\langle (p^2 - 1)/2 \rangle$ multiplied by the local concentration (volume density) of solvent molecules $n = n(x)$ then measures the entropy contribution to the free energy cost related to ordering the solvent molecules along the x-axis. The third term in eq 1 enforces the normalization $\langle p \rangle = 1$ through a Lagrange multiplier λ. The fourth term in eq 1 describes the ability of the lipid headgroups to order the solvent molecules. Water molecules that instead of engaging in hydrogen bonds with other water molecules do so with the lipid, are subject to a lipid-induced orientational ordering. This can arise from interactions of water with any lipid part, including the ester and carbonyl groups. For simplicity, we assume that the ordering potential can be described by a single constant, a dimensionless ordering strength α that couples the first moment $\langle sp \rangle$ of the orientational probability distribution p to the change in solvent density n' along the x-direction. Because the coupling results from the presence of the lipid headgroups, we expect it to grow with the headgroup density $1/a$. This rationalizes the presence of the Chapman length $l_C = a/4\pi l_B$ in the denominator of the coupling term. The final integral in eq 1 corresponds to the linearized ideal mixing free energy of the electrolyte's positive and negative mobile salt ions, respectively. Local salt cation and anion concentrations are $n_+ = n_+(x)$ and $n_- = n_-(x)$, respectively, and the bulk concentration is $n_0 = n_+(x \to \infty) = n_-(x \to \infty)$. The linearization works well only for small deviations of the local from the bulk concentration. In order to avoid large changes of salt ion concentrations, we exclude them from the headgroup region. Mathematically, this is embodied by the final integral starting at l (instead of 0).

The first moment $\langle sp \rangle$ of the dipole's orientational probability distribution p determines the polarization $P = 2en\langle sp \rangle$. Spatial changes of the polarization $(-P')$, in addition to the positive lipid headgroup charges $[\rho^{hg} = (1 - \phi)e/(al)]$ and salt ions outside the headgroup region $[\rho^{salt} = e(n_+ - n_-)]$, contribute to the total volume charge density $\rho = -P' + \rho^{hg} + \rho^{salt}$, implying

$$\frac{\rho}{e} = -(2n\langle sp \rangle)' + \begin{cases} \dfrac{1 - \phi}{al} & 0 \le x \le l \\ n_+ - n_- & x > l \end{cases} \tag{3}$$

Note that ρ enters Poisson's equation $\Psi'' = -4\pi l_B \rho/e$. At this point, we can functionally minimize the free energy $F = F(p, n_+, n_-)$ in eq 1 (for details, see the Appendix), leading to the equilibrium orientational probability distribution function

$$p = 1 - 2s\left[\Psi' + \alpha \frac{l}{l_C} \frac{n'}{n} \right] \tag{4}$$

and equilibrium salt ion distributions

$$n_\pm = n_0(1 \mp \Psi) \tag{5}$$

Equation 4 can conveniently be re-expressed upon introducing the relative polarization $P_{rel} = P/P_{max} = 2n\langle sp \rangle/(n_W l_W)$, which adopts the value $P_{rel} = 1$ for the maximal polarization $P_{max} = el_W n_W$ of bulk water. Here, $n_W = (1/18)\,\text{mol/cm}^3$ denotes the volume density of bulk water. Expressing the first moment of eq 4 in terms of the relative polarization yields

$$P_{rel} = -\frac{1}{3} \frac{l_W}{n_W}\left(n\Psi' + \alpha \frac{l}{l_C} n' \right) \tag{6}$$

Moreover, inserting the polarization according to eq 6 and the ion distributions according to eq 5 into Poisson's equation leads to

$$\Psi'' = -\frac{4}{3}\pi l_B l_W{}^2\left[n\Psi' + \alpha \frac{l}{l_C} n' \right]'$$
$$+ \begin{cases} -4\pi l_B \dfrac{1 - \phi}{al} & 0 \le x \le l \\ 8\pi l_B n_0 \Psi & x > l \end{cases} \tag{7}$$

The first term on the rhs of eq 7 accounts for the influence of the solvent molecules on the electrostatic potential. The final term on the rhs of eq 7 in the region $0 \le x \le l$ reflects the assumption of a uniform distribution of positive headgroup charges with volume density $(1 - \phi)/al$. The final term on the rhs of eq 7 in the region $x > l$ results from the presence of mobile salt ions.

Outside of the headgroup region ($x > l$), the water density is constant, $n(x) = n_W$, implying that eq 7 can be written in that region as

$$\Psi'' = \frac{8\pi l_B n_0}{1 + (4/3)\pi l_B l_W{}^2 n_W}\Psi \tag{8}$$

This simply represents the Debye–Hückel equation in a salt solution of Debye screening length $1/\kappa$ with $\kappa^2 = 8\pi l_B^W n_0$, where $l_B^W = l_B/\varepsilon_W$ is the Bjerrum length in water and ε_W the dielectric constant of bulk water. Comparison of $\Psi'' = \kappa^2\Psi$ with eq 8 yields

$$\varepsilon_W = 1 + \frac{4}{3}\pi l_B l_W{}^2 n_W \tag{9}$$

for the solvent's dielectric constant.[47] Note that in the linear Debye–Hückel limit the dielectric constant is independent of the local electric field; in the nonlinear PB regime, this is no longer the case.[47] Liquid water has a molecular volume of $1/n_W = 0.03\,\text{nm}^3$. Together with the previously introduced quantities $l_B = 56\,\text{nm}$ and $l_W = 0.1\,\text{nm}$, we thus reproduce from eq 9 the dielectric constant of water $\varepsilon_W = 80$ and its Bjerrum length $l_B^W = 0.7\,\text{nm}$. Note that ε_W in eq 9 has a similar structure as in Kirkwood's equation for the bulk dielectric constant, which explicitly takes into account interactions between water molecules.[57] Our present approach lumps these interactions into the properties (that is, into the dipole moment $p_w = el_W$) of each individual solvent molecule.

After calculating the dielectric constant ε_W of bulk water, we address the local dielectric constant (that is, its component along the x-direction) within the headgroup region. From the general relation between polarization $\mathbf{P} = (\varepsilon - 1)\varepsilon_0\mathbf{E}$ and electric field $\mathbf{E}$, we find the position-dependent dielectric constant.

$$\varepsilon(x) = 1 - 4\pi l_B l_W n_W \frac{P_{rel} - P_{rel}^{ref}}{\Psi'} \tag{10}$$

where the term $P_{rel} - P_{rel}^{ref}$ takes into account only the electrostatic contribution to the relative polarization. That is, P_{rel}^{ref} is the polarization of the water molecules induced by the ordering of the lipid headgroups in the absence of an electric field. Below, in eq 18, we calculate $\varepsilon(x)$ using eq 10.

In order to proceed, it is useful to specify the water density inside the headgroup region. (In eq 8, we have already used the assumption that $n(x > l) = n_W$ is constant.) Note that our

model does not attempt to calculate this density. Instead, we make the most simple (but physically reasonable) assumption of imposing a linear function.

$$n(x) = n_W \begin{cases} \dfrac{x}{l} & 0 \leq x \leq l \\ 1 & x > l \end{cases} \tag{11}$$

That is, the density of water increases from $n(x = 0) = 0$ to its bulk value $n(x = l) = n_W$ in a linear manner and then stays constant outside the headgroup region.

Consider now eq 7 inside the headgroup region, $0 \leq x \leq l$. To solve this differential equation, we need to specify two boundary conditions. The first boundary condition follows from the first integral of eq 7 in the vicinity of $x = 0$.

$$\Psi'(0) = -(\varepsilon_W - 1)\frac{\alpha}{l_C} + \frac{1}{l_C} \tag{12}$$

The second boundary condition follows from the first integral of eq 7 in the vicinity of $x = l$.

$$-\kappa\Psi(l) - \Psi'(l) = \frac{\varepsilon_W - 1}{\varepsilon_W}\frac{\alpha}{l_C} \tag{13}$$

Using our definitions for $n(x)$, ε_W, and κ, we can rewrite eq 7 inside the headgroup region as

$$\Psi'' = \frac{(1 - \varepsilon_W)}{l}(\Psi' + x\Psi'') - \frac{1 - \phi}{l_C l} \tag{14}$$

Subject to the boundary conditions in eqs 12 and 13, the solution of eq 14 in the region $0 \leq x \leq l$ is

$$\Psi(x) = -\frac{\phi}{l_C \kappa \varepsilon_W} + \frac{(1 - \phi)(l - x)}{l_C(\varepsilon_W - 1)}$$
$$- \frac{l}{l_C}\left[\alpha - \frac{\varepsilon_W - \phi}{(\varepsilon_W - 1)^2}\right]\ln\left[\frac{1}{\varepsilon_W} + \left(1 - \frac{1}{\varepsilon_W}\right)\frac{x}{l}\right] \tag{15}$$

Note that outside the headgroup region the potential fulfills the classical Debye–Hückel equation $\Psi''(x) = \kappa^2\Psi$ (see eq 8 and the discussion thereafter) and, in addition, must be continuous at $x = l$. From this, we find $\Psi(x) = \Psi(l)\exp[-\kappa(x - l)]$, where $\Psi(l) = -\phi/\varepsilon_W \kappa l_C$ is the potential at the interface between the headgroup region and the aqueous phase. On the basis of eq 15, we calculate the dipole potential as the potential difference $\Psi_{dip} = \Psi(x = 0) - \Psi(l)$ across the headgroup region

$$\Psi_{dip} = \frac{l}{l_C}\left\{\frac{1 - \phi}{\varepsilon_W - 1} + \left[\alpha - \frac{\varepsilon_W - \phi}{(\varepsilon_W - 1)^2}\right]\ln \varepsilon_W\right\} \tag{16}$$

Besides the dipole potential, we are also able to specify other structural quantities such as the relative polarization P_{rel} of the solvent across the headgroup region. Inserting the linear water density profile (eq 11) into eq 6 and using eq 15 yields

$$P_{rel} = -\frac{l_W}{3l_C}\frac{\alpha + \frac{x}{l} - (1 - \phi)\left(\frac{x}{l}\right)^2}{1 + (\varepsilon_W - 1)\frac{x}{l}} \tag{17}$$

implying $P_{rel}(x = 0) = -\alpha l_W/(3l_C)$ and $P_{rel}(x = l) = -(\alpha + \phi) l_W/(3l_C \varepsilon_W)$. Hence, for $\phi = 0$, the relative polarization drops by a factor of ε_W when crossing the zwitterionic headgroups starting at the hydrocarbon chain region. In addition, for the

dielectric constant $\varepsilon(x)$ inside the headgroup region, $0 \leq x \leq l$, we obtain from eqs 10, 15, and 17 the linear relation.

$$\varepsilon(x) = 1 + \frac{x}{l}(\varepsilon_W - 1) \tag{18}$$

As discussed above (see eq 9), outside the headgroup region ($x > l$), we have a constant $\varepsilon(x) = \varepsilon_W$. The dielectric constant inside the headgroup region reflects the water density; there is no influence of α because the nature of the lipid-induced ordering strength is nonelectrostatic.

■ RESULTS AND DISCUSSION

Our theoretical model yields analytical expressions for the electrostatic properties across a lipid layer. In the following, we analyze these properties. Figure 3 shows numerical examples
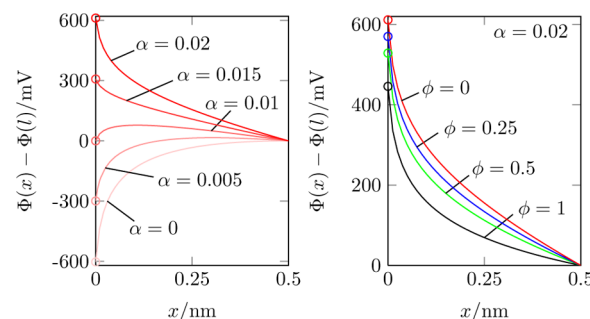
Figure 3. Electrostatic potential $\Phi(x) - \Phi(l)$ according to eq 15 with $\Phi = \Psi \cdot k_B T/e = \Psi \cdot 25$ mV as a function of the distance x from the apolar/polar surface. Left diagram: only zwitterionic lipids are present ($\phi = 0$), and different curves refer to different ordering strengths as indicated. Right diagram: $\alpha = 0.02$, and different curves refer to different mole fractions ϕ of DMPA as indicated. All curves in both diagrams are plotted for fixed $\varepsilon_W = 80$, $l_B = 56$ nm, $a = 0.65$ nm², and $l = 0.5$ nm.

for the electrostatic potential across the lipid layer, $\Phi(x) - \Phi(l)$ according to eq 15 with $\Phi = \Psi k_B T/e$, displayed for a headgroup thickness of $l = 0.5$ nm and a lateral cross-sectional area per lipid of $a = 0.65$ nm². The left diagram of Figure 3 corresponds to a pure zwitterionic lipid layer ($\phi = 0$) and five different values of the ordering strength α. Note that the potential $\Psi(x)$ vanishes outside the headgroup region $x > 0$. For small α, the electrostatic potential is negative. Here, the contribution of the ordered solvent molecules to the dipole potential is insufficient to compensate the negative dipole potential that originates from the lipid's intrinsic P⁻–N⁺ dipole. However, above a certain value of α, lipid-induced water ordering induces a positive potential. The latter corresponds to the mechanism suggested by analyzing MD simulation data.[29] The right diagram of Figure 3 exemplifies the influence of adding anionic lipid (increasing ϕ). The upper red lines in both the left and right diagrams of Figure 3 are identical and correspond to the same zwitterionic layer ($\phi = 0$ with $\alpha = 0.02$). Adding the anionic lipid (the blue line for $\phi = 0.25$, the green line for $\phi = 0.5$, and the black line for $\phi = 1.0$) renders the potential less positive because the anionic lipids contribute only a negatively charged phosphate group (P⁻) instead of a P⁻–N⁺ dipole to the lipid headgroup region.

As mentioned above, classical PB theory[35,36] is based on treating the solvent as a dielectric background. The classical model cannot explain the positive potential inside a lipid layer, because it ignores specific lipid–solvent interactions. Indeed, if

we ignore the lipid-induced ordering of the solvent ($\alpha = 0$), the dipole potential Ψ_{dip} in eq 16 is always negative, irrespective of the composition ϕ. In order to obtain a positive dipole potential Ψ_{dip}, the water ordering strength α needs to be larger than a certain critical value α_c. Equation 16 yields the condition

$$\alpha > \alpha_c = \frac{\varepsilon_W - \phi}{(\varepsilon_W - 1)^2} - \frac{1 - \phi}{\varepsilon_W - 1}\frac{1}{\ln \varepsilon_W} \tag{19}$$

For a zwitterionic layer ($\phi = 0$) and $\varepsilon_W = 80$, the numerical value is $\alpha_c = 0.01$.

Recall that the right diagram in Figure 1 contains our experimental data for the dipole potential Φ_{dip} of a mixed DMPC/DMPA monolayer with mole fractions $\phi = 0$, $\phi = 0.25$, $\phi = 0.5$, and $\phi = 1.0$ of DMPA. On the other hand, eq 16 is our theoretical prediction for the dipole potential $\Psi_{dip} = e\Phi_{dip}/k_BT$. Figure 4 shows a comparison of the two, the experimental

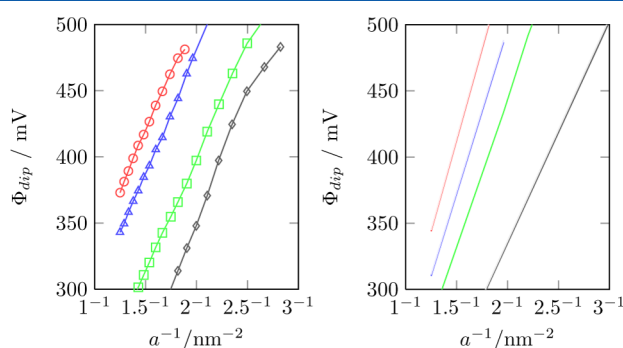**Figure 4.** Dipole potential Φ_{dip} of a mixed DMPC/DMPA monolayer as a function of the inverse cross-sectional area a^{-1} per lipid. Different curves refer to different mole fractions ϕ of DMPA: $\phi = 0$ (red curve), $\phi = 0.25$ (blue curve), $\phi = 0.5$ (green curve), and $\phi = 1$ (black curve). The left diagram displays experimental data, whereas the right diagram corresponds to our theoretical predictions according to eq 16. All curves refer to fixed $\alpha = 0.02$, $\varepsilon_W = 80$, $l_B = 56$ nm, and $l = 0.5$ nm.

results and theoretical prediction in the left and right diagrams, respectively. According to eq 16, we have $\Psi_{dip} \sim 1/l_C$ with $l_C = a/4\pi l_B$. Hence, it is convenient to plot Φ_{dip} in Figure 4 as a function of the inverse cross-sectional area $1/a$, yielding straight lines in the right diagram. To produce the right diagram in Figure 4, we have chosen $\Phi_{dip} = \Psi_{dip}\cdot 25$ mV (valid for room temperature), $\varepsilon_W = 80$ (the dielectric constant of bulk water), $l = 0.5$ nm (the headgroup thickness), $l_B = 56$ nm (the Bjerrum length in vacuum at room temperature), and $\alpha = 0.02$ (the lipid-induced ordering strength of the solvent). Note that only α is an unknown interaction parameter that we have chosen so as to obtain best agreement between the left and right diagrams in Figure 4. The value $\alpha = 0.02$ is twice $\alpha_c = 0.01$ for the zwitterionic case; see eq 19 and Figure 3.

We can simplify the expression for the dipole potential further. First, the expression for Ψ_{dip} in eq 16 is, in principle, valid for any value of the solvent's dielectric constant. Assuming $\varepsilon_W \gg 1$ yields the following approximative expression for the dipole potential.

$$\Psi_{dip} = \frac{l}{\varepsilon_W l_C}[1 - \phi + (\varepsilon_W \alpha - 1)\ln \varepsilon_W] \tag{20}$$

Second, we can make use of the fact that the experimental data are fitted best for $\alpha = 2\alpha_c$ with

$$\alpha_c = \frac{1}{\varepsilon_W}\left(1 - \frac{1}{\ln \varepsilon_W}\right) \tag{21}$$

valid for $\phi = 0$ and $\varepsilon_W \gg 1$. (Specifically, for $\varepsilon_W = 80$, we obtain $\alpha_c = 0.01$; the corresponding potential $\Psi(x)$ for $\alpha = \alpha_c$ is shown in the left diagram of Figure 3, middle curve.) Upon inserting $\alpha = 2\alpha_c$ with eq 21 into eq 20, we obtain $\Psi_{dip} = l (\ln \varepsilon_W - 1 - \phi)/(\varepsilon_W l_C)$. Third, using the definitions for $l_C = a/(4\pi l_B)$, $l_B = e^2/(4\pi\varepsilon_0 k_BT)$, and $\Psi = e\Phi/k_BT$, we can express Φ_{dip} as

$$\Phi_{dip} = \frac{1}{a}\frac{el}{\varepsilon_W \varepsilon_0}(\ln \varepsilon_W - 1 - \phi) \tag{22}$$

This is an explicit expression in terms of fundamental quantities for the dipole potential Φ_{dip} that describes our experimental data as a function of a and ϕ. The slopes of the linear functions $\Phi_{dip} = \Phi_{dip}(1/a)$ depend only on the dielectric constant of water ε_W, on the mole fraction ϕ, and on the headgroup thickness l.

The lipid layer can be described as a parallel-plate capacitor with capacitance per unit area

$$c = \frac{q}{\Phi_{dip}} = \varepsilon_0 \varepsilon_{eff}\frac{1}{l} \tag{23}$$

where $q = e/a$ is the magnitude of the charge density on each of the two plates, l is the distance between the plates, and ε_{eff} is the effective dielectric constant inside the capacitor. A comparison with eq 22 yields for the effective dielectric constant

$$\varepsilon_{eff} = \frac{\varepsilon_W}{\ln \varepsilon_W - 1 - \phi} \tag{24}$$

With $\varepsilon_W = 80$, our model predicts an effective dielectric constant in the headgroup region that increases from $\varepsilon_{eff} = 23$ for a zwitterionic lipid layer ($\phi = 0$) to $\varepsilon_{eff} = 33$ for an anionic lipid layer ($\phi = 1$). We point out that this estimate depends on the composition ϕ and is smaller than the spatial average $(1 + \varepsilon_W)/2 \approx 40$ of the local dielectric constant $\varepsilon(x)$ in eq 18. In fact, our prediction for ε_{eff} agrees well with a more detailed theoretical prediction ($\varepsilon_{eff} \approx 23$–29 for a zwitterionic lipid) by Raudino and Mauzerall.[58]

Our model is intentionally made as simple as possible so as to highlight the overcompensation of the lipid's intrinsic dipole potential by that of the solvent molecules. Consequently, our approach involves a range of approximations, including the mean-field nature of treating electrostatic interactions, lateral averaging over the lipids, linearizing the free energy, excluding salt ions from the headgroup region, representing the solvent by dipoles that only interact through an external electrostatic field, neglecting all higher order moments of the solvent, ignoring the contribution of the terminal methyl groups to the dipole potential, and assuming both a linear change of solvent concentration across the headgroup region and a constant ordering strength of the solvent induced by the headgroups. Some of our approximations deserve further commenting:

First, our approach of modeling the solvent corresponds to the linearized version of representing each solvent molecule by a Langevin dipole,[47−49,51,59] where the dipoles interact with the electrostatic field $-\Phi' = -k_BT\Psi'/e$ and with an additional nonelectrostatic lipid−solvent interaction embodied in the ordering strength α. In the nonlinear approach, the Langevin dipoles would adopt a relative polarization $P_{rel} = -\mathcal{L}(l_W\Psi' + l_W\alpha n'/n)$, where $\mathcal{L}(x) = \coth x - 1/x$ is the Langevin function.

Linearization of the Langevin function requires the argument $|l_W\Psi' + l_W\alpha n'/n|$ to be sufficiently small. For $\alpha = 0.01$, the potential (and its first derivative) becomes small (see the left diagram of Figure 3) and linearization is justified. For the extreme cases $\alpha = 0$ and $\alpha = 0.02$, linearization still works, apart from the immediate vicinity of $x = 0$. For example, $|l_W\Psi' + l_W\alpha n'/n| > 3$ for $x < 0.1$ nm at $\alpha = 0.02$. Hence, at least on a qualitative level, linearization of the solvent response is a reasonable approach.

Second, when ionic systems embedded in an aqueous solution of monovalent counterions and co-ions are described within PB theory, linearization (Debye–Hückel approximation) is applicable as long as the magnitude of the electrostatic energy remains comparable to that of the thermal energy ($\Psi \lesssim 1$). In the present work, the potential becomes large but only within the lipid headgroup region. By excluding salt ions from the headgroup region, we can not only justify linearization of the PB model but also find a simple analytical solution for the potential.

Third, more than 70 years ago, Kirkwood[57] developed a theory that considers correlations between the orientations of neighboring water molecules. The bulk dielectric constant that follows from Kirkwood's theory is $\varepsilon = 1 + 6\pi n_W(1 + z\langle\cos\gamma\rangle) p_W^2/(3k_BT)$, where p_w is the dipole moment of a water molecule, z is a lattice coordination number, and $\langle\cos\gamma\rangle$ describes the orientation-dependent interaction strength between neighboring water molecules. As mentioned above, our approach lumps these interactions into the dipole moment $p_w = el_W$ (note that water–water interactions can also be included explicitly into the present model[59]).

Fourth, the lipid chains carry partial charges also on the terminal methyl groups. In the case of lipid bilayers (but not for lipid monolayers), the corresponding electrostatic contributions partially cancel each other. For a lipid monolayer, we estimate the contribution of the terminal methyl groups to the dipole potential using a simple capacitor model. To this end, we introduce a capacitor that describes the partial charges on the terminal methyl group of a lipid tail, with a capacitance per unit area $C = \varepsilon_0\varepsilon_c/(\delta\chi)$, where $\delta \approx 0.02$ nm is the thickness of a methyl group and $\varepsilon_c = 5$ the dielectric constant within the hydrocarbon chain region. The order parameter χ describes changes of the average chain orientation. For fully stretched chains $\chi = 1$, whereas for disordered chains in the fluid state $\chi \approx 0.50$. The contribution of the terminal methyl group layer to the potential is $\Phi_c = 2e\delta\chi/(a\varepsilon_0\varepsilon_c)$, where the prefactor of 2 applies to lipids with two hydrocarbon tails. This potential difference can be compared to the potential difference of the capacitor describing the headgroup region (the capacitance per unit area of which is given in eq 23): $\Phi_{dip} = el/(a\varepsilon_0\varepsilon_{eff})$. From calculating the ratio $\Phi_c/\Phi_{dip} = 2\delta\chi\varepsilon_{eff}/(l\varepsilon_c) \approx 0.2\chi$, we estimate that Φ_c contributes about 10−20% to the dipole potential of a lipid monolayer, assuming $0.5 \lesssim \chi \leq 1$.

CONCLUSION

To conclude, detailed computer simulations suggest that the physical mechanism leading to the positive dipole potential across a lipid layer is the result of an overcompensation of the bare lipid's negative electrostatic potential by a positive contribution from ordered solvent molecules. The present work lumps these two opposing tendencies into an analytic model that is based on continuum electrostatics and explicit modeling of the solvent molecules as orientationally mobile dipoles. Our main result is an explicit and simple expression for

the dipole potential; see eq 22. Comparison of this expression with the measured dipole potential of a mixed anionic–zwitterionic monolayer at the air–water interface indicates excellent agreement, both as a function of the monolayer composition and average cross-sectional area per lipid. Given the qualitative nature of our model, its ability to reproduce our experimental data is notable.

APPENDIX

In order to find the unknown orientational probability distribution function, the electrostatic potential, and the ion distributions, we calculate the first variation of the free energy (eq 1).

$$\frac{\delta F}{Ak_BT} = \int_0^\infty dx \frac{(\Psi\delta\Psi')' - \Psi\delta\Psi''}{4\pi l_B}$$
$$+ \int_0^\infty dx\langle(np + \lambda)\delta p\rangle + \alpha\frac{2l}{l_C}\int_0^l dx\langle s\delta p\rangle n'$$
$$+ \int_l^\infty dx\left\{\frac{n_+}{n_0}\delta n_+ - \delta n_+ + \frac{n_-}{n_0}\delta n_- - \delta n_-\right\}$$

(25)

The term $1/(4\pi l_B)\int_0^\infty dx(\Psi\delta\Psi')'$ can be integrated, resulting in the expression $-\Psi(0)\delta\Psi'(0)/(4\pi l_B)$. Taking into account the first variation of the boundary condition at $x = 0$ (eq 12) yields

$$-\frac{1}{4\pi l_B}\int_0^\infty dx(\Psi\delta\Psi')' = -\Psi(0)\delta\left[\frac{1}{a} + 2n\langle sp\rangle\right]$$

(26)

We rewrite the term $-1/(4\pi l_B)\int_0^\infty dx\Psi\delta\Psi''$ in eq 25 using the first variation of Poisson's equation $\delta\Psi'' = -4\pi l_B\delta\rho/e$, where ρ is the total volume charge density specified by eq 3, and obtain $-\int_0^\infty dx\Psi[(2n\langle s\delta p\rangle)' + \delta n_+ - \delta n_-]$. After a partial integration, this becomes

$$-\frac{1}{4\pi l_B}\int_0^\infty dx\Psi\delta\Psi''$$
$$= -\int_0^\infty dx\{[\Psi 2n\langle s\delta p\rangle]' - \Psi'2n\langle s\delta p\rangle\}$$
$$+ \int_0^\infty dx\{\delta n_+ - \delta n_-\}$$

(27)

Inserting eqs 26 and 27 into eq 25 results in

$$\frac{\delta F}{Ak_BT} = -\Psi(0)\delta\left[\frac{1}{a} + 2n\langle sp\rangle\right] + \Psi(0)2n\langle s\delta p\rangle$$
$$+ \int_0^\infty dx\left\langle\left(np + \lambda + \alpha\frac{2l}{l_C}n's + \Psi'2ns\right)\delta p\right\rangle$$
$$+ \int_l^\infty dx\left\{\delta n_+\left(\Psi + \frac{n_+}{n_0} - 1\right)\right.$$
$$\left. + \delta n_-\left(-\Psi + \frac{n_-}{n_0} - 1\right)\right\}$$

(28)

Thermal equilibrium demands $\delta F = 0$. Note that the expression in the first line of eq 28 vanishes because the n-dependent contributions cancel each other and because the cross-sectional area a per lipid is fixed (implying $\delta a = 0$). From the vanishing of the first and second integrals in eq 28, the orientational

probability distribution function (eq 4) and the equilibrium ion distributions (eq 5) follow.

■ AUTHOR INFORMATION

Corresponding Author

*E-mail: klemen.bohinc@zf.uni-lj.si. Phone: +386 1300 1170. Fax: +386 1300 1119.

Notes

The authors declare no competing financial interest.

■ REFERENCES

(1) Liberman, Y. A.; Topaly, V. P. Permeability of bimolecular phospholipid membranes for fat-soluble ions. *Biophysics* **1969**, *14*, 477−487.

(2) LeBlanc, O. Single ion conductances in lipid bilayers. *Biophys. J.* **1970**, *14*, 94a.

(3) Dynarowicz-Latka, P.; Dhanabalan, A.; Olivera, O. N. Modern physicochemical research on Langmuir monolayers. *Adv. Colloid Interface Sci.* **2001**, *91*, 221−293.

(4) Wang, L. G. Measurements and implications of the membrane dipole potential. *Annu. Rev. Biochem.* **2012**, *81*, 615−635.

(5) Haydon, D. A.; Hladky, S. B. Ion transport across thin lipid membranes: a critical discussion of mechanisms in selected systems. *Q. Rev. Biophys.* **1972**, *5*, 187−192.

(6) Simon, S. A.; McIntosh, T. J. Magnitude of the solvation pressure depends on the dipole potential. *Proc. Natl. Acad. Sci. U.S.A.* **1989**, *86*, 9263−9267.

(7) McLaughlin, S. In *Electrostatic potentials at membrane-solution interfaces*; Bronner, F., Kleinzeller, A., Eds.; Academic Press: New York, 1977; Vol. 9, pp 1−144.

(8) Honig, B. H.; Hubbell, W. L.; Flewelling, R. F. Electrostatic interactions in membranes and proteins. *Annu. Rev. Biophys. Biophys. Chem.* **1986**, *15*, 163−193.

(9) Clarke, R. J. Effect of lipid structure on the dipole potential of phosphatidylcholine bilayers. *Biochim. Biophys. Acta, Biomembr.* **1997**, *1327*, 269−278.

(10) Peterson, U.; Mannock, D. A.; Lewis, R. N. A. H.; Pohl, P.; McElhaney, R. N.; Pohl, E. E. Origin of membrane dipole potential: Contribution of the phospholipid fatty acid chains. *Chem. Phys. Lipids* **2002**, *117*, 19−27.

(11) Horinek, D.; Herz, A.; Vrbka, L.; Sedlmeier, F.; Mamatkulov, S. I.; Netz, R. R. Specific ion adsorption at the air/water interface: The role of hydrophobic solvation. *Chem. Phys. Lett.* **2009**, *479*, 173−183.

(12) Clarke, R. The dipole potential of phospholipid membranes and methods for its detection. *Adv. Colloid Interface Sci.* **2001**, *89*, 263−281.

(13) Milhaud, J. New insights into water-phospholipid model membrane interactions. *Biochim. Biophys. Acta, Biomembr.* **2004**, *1663*, 19−51.

(14) Smaby, J.; Brockman, H. Surface dipole-moments of lipids at the argon-water interface-similarities among glycerol-ester-based lipids. *Biophys. J.* **1990**, *58*, 195−204.

(15) Flewelling, R. F.; Hubbell, W. L. The membrane dipole potential in a total membrane-potential model - applications to hydrophobic ion interactions with membranes. *Biophys. J.* **1986**, *49*, 541−552.

(16) Becucci, L.; Moncelli, M.; Herrero, R.; Guidelli, R. Dipole potentials of monolayers of phosphatidylcholine, phosphatidylserine, and phosphatidic acid on mercury. *Langmuir* **2000**, *16*, 7694−7700.

(17) Yang, Y.; Mayer, K. M.; Wickremasinghe, N. S.; Hafner, J. H. Probing the lipid membrane dipole potential by atomic force microscopy. *Biophys. J.* **2008**, *95*, 5193−5199.

(18) Gawrisch, K.; Ruston, D.; Zimmerberg, J.; Parsegian, V.; Rand, R.; Fuller, N. Membrane dipole potentials, hydration forces, and the ordering of water at membrane surfaces. *Biophys. J.* **1992**, *61*, 1213−1223.

(19) Wang, L.; Bose, P. S.; Sigworth, F. J. Using cryo-EM to measure the dipole potential of a lipid membrane. *Proc. Natl. Acad. Sci. U.S.A.* **2006**, *103*, 18528−18533.

(20) Zhou, F.; Schulten, K. Molecular-dynamics study of a membrane water interface. *J. Phys. Chem.* **1995**, *99*, 2194−2207.

(21) Feller, S.; Pastor, R.; Rojnuckarin, A.; Bogusz, S.; Brooks, B. Effect of electrostatic force truncation on interfacial and transport properties of water. *J. Phys. Chem.* **1996**, *100*, 17011−17020.

(22) Saiz, L.; Klein, M. Electrostatic interactions in a neutral model phospholipid bilayer by molecular dynamics simulations. *J. Chem. Phys.* **2002**, *116*, 3052−3057.

(23) Smondyrev, A.; Berkowitz, M. United atom force field for phospholipid membranes: Constant pressure molecular dynamics simulation of dipalmitoylphosphatidicholine/water system. *J. Comput. Chem.* **1999**, *20*, 531−545.

(24) Mojumdar, E. H.; Lyubartsev, A. P. Molecular dynamics simulations of local anesthetic articaine in a lipid bilayer. *Biophys. Chem.* **2010**, *153*, 27−35.

(25) Zheng, C.; Vanderkooi, G. Molecular-origin of the internal dipole potential in lipid bilayers - calculation of the electrostatic potential. *Biophys. J.* **1992**, *63*, 935−941.

(26) Gabdoulline, R. R.; Zheng, C.; Vanderkooi, G. Molecular origin of the internal dipole potential in lipid bilayers: Role of the electrostatic potential of water. *Chem. Phys. Lipids* **1996**, *84*, 139−146.

(27) Lin, J. H.; Baker, N. A.; McCammon, J. A. Bridging implicit and explicit solvent approaches for membrane electrostatics. *Biophys. J.* **2002**, *83*, 1374−1379.

(28) Brockman, H. Dipole potential of lipid-membranes. *Chem. Phys. Lipids* **1994**, *73*, 57−79.

(29) Berkowitz, M. L.; Bostick, D. L.; Pandit, S. Aqueous solutions next to phospholipid membrane surfaces: Insights from simulations. *Chem. Rev.* **2006**, *106*, 1527−1539.

(30) Essmann, U.; Berkowitz, M. Dynamical properties of phospholipid bilayers from computer simulation. *Biophys. J.* **1999**, *76*, 2081−2089.

(31) Mashl, R.; Scott, H.; Subramaniam, S.; Jakobsson, E. Molecular simulation of dioleoylphosphatidylcholine lipid bilayers at different levels of hydration. *Biophys. J.* **2001**, *81*, 3005−3015.

(32) Marrink, S. J.; Tieleman, D. P.; vanBuuren, A. R.; Berendsen, H. J. C. Membranes and water: An interesting relationship. *Faraday Discuss.* **1996**, *103*, 191−201.

(33) Stern, H. A.; Feller, S. E. Calculation of the dielectric permittivity profile for a nonuniform system: Application to a lipid bilayer simulation. *J. Chem. Phys.* **2003**, *118*, 3401−3412.

(34) Peitzsch, R. M.; Eisenberg, M.; Sharp, K. A.; M, S. Calculations of the electrostatic potential adjacent to model phospholipid bilayers. *Biophys. J.* **1995**, *68*, 729−738.

(35) McLaughlin, S. The electrostatic properties of membranes. *Annu. Rev. Biophys. Biophys. Chem.* **1989**, *18*, 113−136.

(36) Cevc, G. Membrane electrostatics. *Biochim. Biophys. Acta* **1990**, *1031*, 311−382.

(37) Murray, D.; Arbuzova, A.; Hangyás-Mihályné, G.; Gambhir, A.; Ben-Tal, N.; Honig, B.; McLaughlin, S. Electrostatic properties of membranes containing acidic lipids and adsorbed basic peptides: theory and experiment. *Biophys. J.* **1999**, *77*, 3176−3188.

(38) Kessel, A.; Cafiso, D. S.; Ben-Tal, N. Continuum solvent model calculations of alamethicin-membrane interactions: thermodynamic aspects. *Biophys. J.* **2000**, *78*, 571−583.

(39) Andelman, D. In *Structure and Dynamics of Membranes*, 2nd ed.; Lipowsky, R., Sackmann, E., Eds.; Elsevier: Amsterdam, The Netherlands, 1995; Vol. 1, Chapter 12, pp 603−642.

(40) Manning, G. S. Limiting laws and counterion condensation in polyelectrolyte solutions. I. Colligative properties. *J. Chem. Phys.* **1969**, *51*, 924−933.

(41) Harries, D.; May, S.; Ben-Shaul, A. Counterion release in membrane-biopolymer interactions. *Soft Matter* **2013**, *9*, 9268−9284.

(42) Vlachy, V. Ionic effects beyond Poisson-Boltzmann theory. *Annu. Rev. Phys. Chem.* **1999**, *50*, 145−165.

(43) Mbamala, E. C.; Fahr, A.; May, S. Electrostatic model for mixed cationic-zwitterionic lipid bilayers. *Langmuir* **2006**, *22*, 5129−5136.

(44) Mengistu, D. H.; May, S. Nonlinear Poisson-Boltzmann model of charged lipid membranes: Accounting for the presence of zwitterionic lipids. *J. Chem. Phys.* **2008**, *129*, 121105−121108.

(45) Gerami, R.; Bruinsma, R. F. Continuum theory of lipid bilayer electrostatics. *Eur. Phys. J. E* **2009**, *30*, 197−204.

(46) Ruckenstein, E.; Manciu, M. The coupling between the hydration and double layer interactions. *Langmuir* **2002**, *18*, 7584−7593.

(47) Abrashkin, A.; Andelman, D.; Orland, H. Dipolar Poisson-Boltzmann equation: Ions and dipoles close to charge interfaces. *Phys. Rev. Lett.* **2007**, *99*, 077801−077804.

(48) Azuara, C.; Orland, H.; Bon, M.; Koehl, P.; Delarue, M. Incorporating dipolar solvents with variable density in Poisson-Boltzmann electrostatics. *Biophys. J.* **2008**, *95*, 5587−5605.

(49) Koehl, P.; Orland, H.; Delarue, M. Beyond the Poisson-Boltzmann model: Modeling biomolecule-water and water-water interactions. *Phys. Rev. Lett.* **2009**, *102*, 087801−087804.

(50) Paillusson, F.; Blossey, R. Slits, plates, and Poisson-Boltzmann theory in a local formulation of nonlocal electrostatics. *Phys. Rev. E* **2010**, *82*, 052501−052504.

(51) Levy, A.; Andelman, D.; Orland, H. Dielectric constant of ionic solutions: A field-theory approach. *Phys. Rev. Lett.* **2012**, *108*, 227801−227804.

(52) Brezesinski, G.; Möhwald, H. Langmuir monolayers to study interactions at model membrane surfaces. *Adv. Colloid Interface Sci.* **2003**, *100*, 563−584.

(53) Kouaouci, R.; Silvius, J.; Graham, I.; Pezolet, M. Calcium-induced lateral phase separations in phosphatidylcholine-phosphatidic acid mixtures - A Raman-spectroscopic study. *Biochemistry* **1985**, *24*, 7132−7140.

(54) Garidel, P.; Blume, A. Calcium induced nonideal mixing in liquid-crystalline phosphatidylcholine-phosphatidic acid bilayer membranes. *Langmuir* **2000**, *16*, 1662−1667.

(55) Garidel, P.; Johann, C.; Blume, A. Nonideal mixing and phase separation in phosphatidylcholine phosphatidic acid mixtures as a function of acyl chain length and pH. *Biophys. J.* **1997**, *72*, 2196−2210.

(56) Mengistu, D. H.; May, S. Debye-Huckel theory of mixed charged-zwitterionic lipid layers. *Eur. Phys. J. E* **2008**, *26*, 251−260.

(57) Kirkwood, J. K. The dielectric polarization of polar liquids. *J. Chem. Phys.* **1939**, *7*, 911−919.

(58) Raudino, A.; Mauzerall, D. Dielectric-properties of the polar head group region of zwitterionic lipid bilayers. *Biophys. J.* **1986**, *50*, 441−449.

(59) Mengistu, D. H.; Bohinc, K.; May, S. Poisson-Boltzmann model in a solvent of interacting Langevin dipoles. *Eur. Phys. Lett.* **2009**, *88*, 14003−14006.